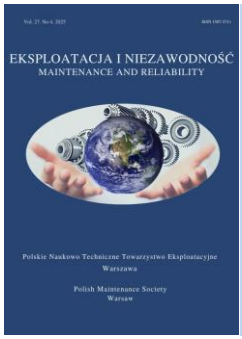

Eksploatacja i Niezawodnosc – Maintenance and Reliability

Volume 27 (2025), Issue 4

journal homepage: http://www.ein.org.pl

Article citation info:
Wieczorek A, Wojnar G, Konieczny Ł, Filipowicz K, Kuczaj M, Pawlikowski A, Zawisza M, Variation analysis of a drive system with an innovative flexible clutch operating under the conditions of constant and cyclically variable load torque of diverse variation waveform, Eksploatacja i Niezawodnosc – Maintenance and Reliability 2025: 27(4) http://doi.org/10.17531/ein/208868

Variation analysis of a drive system with an innovative flexible clutch operating under the conditions of constant and cyclically variable load torque of diverse variation waveform

Indexed by: Web of Science Group

Andrzej Wieczorek[a], Grzegorz Wojnar[b,*], Łukasz Konieczny[b], Krzysztof Filipowicz[a], Mariusz Kuczaj[a], Arkadiusz Pawlikowski[a], Maciej Zawisza[c]

[a] Department of Mining Mechanisation and Robotisation, Silesian University of Technology, Poland
[b] Department of Road Transport, Silesian University of Technology, Poland
[c] Institute of Machine Design Fundamentals, Warsaw University of Technology, Poland

Highlights

- The real-life operating conditions of mining scraper conveyor drive systems.
- Vibrations in the drive system with the innovative flexible damping clutch.
- Test of drive system under cyclically variable load torque.
- Drive system featuring an innovative flexible damping clutch working to 200 angle degree.

Abstract

During machinery operation, load is often highly variable, which exerts an impact on how the machinery service life is reduced; hence the need for decreasing the variations in the load torque affecting the driving elements of machines. In order to achieve such reduction, the authors have developed a flexible clutch of innovative design. This paper provides a follow-up to the studies of the dynamic properties of the said clutch in terms of the analysis of the effect attributable to the input function waveform of the applied load on the dynamic response of the system, represented by the value of the accelerations of the drive system vibrations. The load variants analysed, with values of 500±250 Nm and 750±375 Nm (sinusoidal, triangular, and rectangular waveforms). On account of the fact that the flexible clutch was integrated with the drive system subject to the studies, it was found that the averaged maximum root mean square reductions of vibration accelerations in the measurement direction with the highest vibration accelerations (direction y) came as high as to 56.1%.

Keywords
gears, transport, flexible clutch, vibrations, reduction, time-varying load, sine, triangle, rectangle

This is an open access article under the CC BY license (https://creativecommons.org/licenses/by/4.0/)

1. Introduction

Even though hard coal is being gradually abandoned as an energy carrier across Europe, there are countries which still increase their extraction of this resource. This is why some researchers, including the authors of paper [1], even refer to them using the term *industrial food*. Given the hard coal mining experience of several hundred years typical of the territory of contemporary Poland, local scientists have gained significant competence in the spheres of safety [2] as well as the problems

(*) Corresponding author.
E-mail addresses: A. Wieczorek (ORCID: 0000-0002-8634-7763) andrzej.n.wieczorek@polsl.pl, G. Wojnar (ORCID: 0000-0003-3515-3990) grzegorz.wojnar@polsl.pl, Ł. Konieczny (ORCID: 0000-0002-9501-7651) lukasz.konieczny@polsl.pl, K. Filipowicz (ORCID: 0000-0001-6672-1378) krzysztof.filipowicz@polsl.pl, M. Kuczaj (ORCID: 0000-0001-6893-0309) mariusz.kuczaj@polsl.pl, A. Pawlikowski (ORCID: 0000-0003-0478-6154) arkadiusz.pawlikowski@polsl.pl, M. Zawisza (ORCID: 0000-0001-7777-1768) maciej.zawisza@pw.edu.pl

addressed in paper [3], i.e. *green technologies and mining practice*. It is precisely for the aforementioned long-standing experience in the machinery design, development, and production, based on expertise founded on the real-life operation of mining machines, that Polish enterprises can successfully ride the wave of global trends related to the development of high-quality mining machines. That includes devices which make use of digital technologies at different life cycle stages [4–7]. Bearing the above rationale in mind, it is reasonable to continue scientific research aimed at raising the durability and reliability of mining machinery. Some of the machines commonly operated in hard coal mines are powered mining systems, which include longwall scraper conveyors. A conveyor of this type is composed of an electric motor, a clutch – typically characterised by a small torsion angle of clutch members, a gear transmission, and a main drive wheel with a chain wrapping connector.

The flexible clutch – typically characterised by a small torsion angle of clutch members, a gear transmission, and a main drive wheel with a chain wrapping connector. Scraper conveyors are important because they enable output haulage by moving transversely arranged elements, known as scrapers, which eliminates the need for belts that are exposed to the risk of fire caused by friction [8, 9]. Research is conducted to study modelling of conveyors [10], durability of chains used in underground mining conditions [11], as well as conveyor chain production methods [12]. Prospects for reducing the wear of conveyor components and increasing their reliability are sought in the monitoring of their rectilinearity [13]. Some other elements subject to in-depth analyses are drive systems, and particularly their components such as drive shafts [14–16], couplings [17–19], bearings [20–22], and gear wheels [15, 23–27], while diagnostic methods are developed at the same time to eliminate their operational failures [28, 29]. Paper [30] provides results of a very detailed literature review performed in an attempt to determine the number of references to different problems related to conveyors (mainly belt conveyors). These results have been depicted in a graph showing that the terms "stress analysis", "finite element analysis", and "dynamics of belt during starting and stopping" were, respectively, the second, third, and fourth most frequently analysed notions in the top twenty. The research results addressed in this paper, i.e. findings of analyses of different loads variable in time, prove to be very useful in the context of effective analyses of the aforementioned subjects.

This study focuses in the first place on such components of the assembly in question as gears, bearings, shaped joints, and shafts. They are all exposed to considerable dynamic forces as a consequence of their operation under time-varying loads [31, 32]. It should be emphasised that the components of these transmissions must not only meet specific strength requirements, but must also be characterised by high operational reliability.

Overall, the operational durability and reliability of mining machinery drive systems are not satisfactory. The service life of these transmissions often does not exceed 10,000 hours. Extending their service life to a degree comparable to that of the drive systems used in other industries (i.e. to 30,000–50,000 h) would bring significant savings to mining plants. Therefore, the development process for modern mining machinery and equipment must be based on an assumption that the manufacturing and operating requirements set for drive systems should be raised significantly. The foregoing pertains particularly to the increase in the power of the electric motors installed in the drives of mining machinery, which entails changes not only in the material selection, but also in the design of drive systems.

It should be emphasised that a drive train composed of gear transmissions coupled via clutches with the driving motor and the driven machine altogether form a kinematic system of elastic elements with specific masses. They are excited to vibrate due to a varying load. Such vibrations can be caused by external forcing, where they originate in the motor and/or the driven machine, as well as by some internal sources (Fig. 1), the effect of which is an increase in the load transferred by driving elements. In maintenance-oriented diagnostics, solutions such as machine learning are used [29]. The monitoring and diagnostic systems used with driven machines (also outside the mining industry) are the key components of operational systems, which make it possible to reduce the unreliability of such machines and to improve the reliability of production processes.

However, in the case of mining machinery, and scraper conveyors in particular, it is relatively rare that predictive systems are used to determine the current technical condition. This can be attributed to the considerable load variability caused

by changing mining conditions, e.g. due to rock interlayers in coal seams or lumps of output falling onto the conveyor.

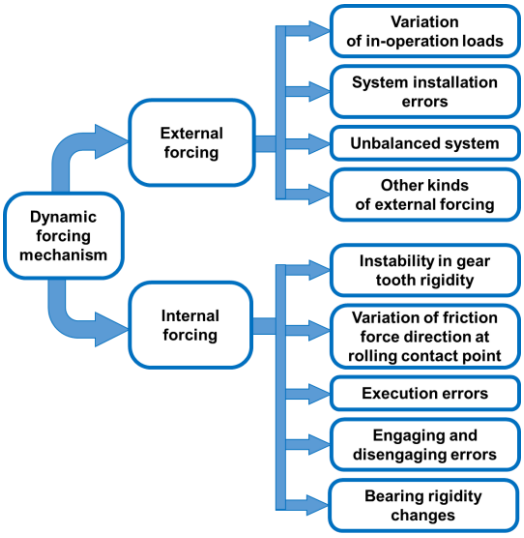

Fig. 1. Causes of gear transmission vibration.

A forces in gear meshing can be minimised by reduction tooth gear deviation [33] and also made to reduce the torque [34–37] caused by the non-constant of the operating conditions of driven machines.

Mechanical couplings are generally used in scraper conveyors, and these are usually flexible insert-type clutches or, less commonly (due to their higher cost), hydrokinetic clutches. The rationale behind using the aforementioned clutches is to improve the alignment of drive shafts and to reduce the dynamic forces caused by frequent start-ups.

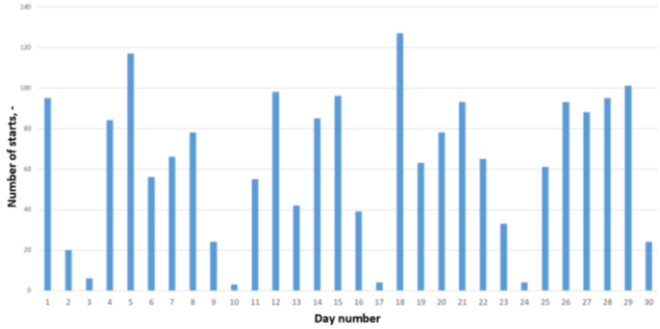

Fig. 2. Summary of the number of start-ups for consecutive days of operation determined for a sample longwall at a hard coal mine; compiled by authors based on [38].

The problem of mining machinery start-up is important in the context of the solutions employed to maintain the durability of mining machine drives. Paper [38] provides a summary of the number of start-ups for consecutive days of mining operation at a sample longwall equipped with a scraper conveyor (Fig. 2). The graph clearly shows that the number of daily start-ups reaches 120, and hence the average number of start-ups per hour of conveyor operation being even as high as 5.

The number of start-ups significantly affects the resultant load acting on the drive elements in mining machinery, since the starting torques emerging in non-linear states considerably exceed the nominal values resulting from the nominal torque value of the driving motor. Some good solutions to minimise external dynamic forces include using hydrokinetic clutches as well as devices referred to as soft-start systems (including subassemblies based on thyristor elements and drive inverters), however, on account of their relatively high cost, they are rarely used in coal mining. It is more common to find solutions based on insert-type clutches and contactor switches in the design of drive systems intended for mining machinery (especially scraper conveyors), even though they do not ensure adequate minimisation of external dynamic forces.

The aforementioned solutions are also unsuitable for reducing the variability of the forces caused by momentary changes in the output-related loading of conveyors as well as by the drive clutch locking.

In order to solve the load variability issue, caused by diverse reasons such as start-ups and locks, the flexible damping clutch was designed, based on a patented solution of a torsionally flexible metal clutch (characterised in detail in publications [39, 40]). Load and vibration tests in drive systems or their components are also important in the case of environmental protection activities [41-42] and operationally oriented diagnostics [43]. This clutch (Fig. 3) is composed of a part being coupled, i.e. an insert-type clutch, and a flexible damping subassembly in which the output member is subject to torsion against the input member, the energy associated with the friction of the screw assembly becomes dissipated, and springs move.

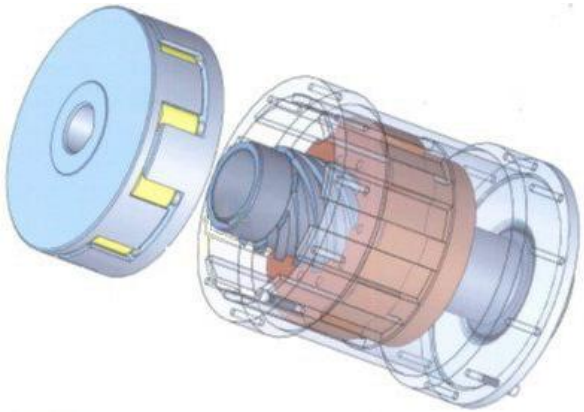

Fig. 3. Design of the flexible damping clutch.

Based on the structure of the flexible clutch described above, a drive system solution was developed, adapted to the requirements of dog heading scraper conveyors (Fig. 4) with 55 kW of power transmitted at n=1,485 RPM of the driving motor speed. The system in question was built and installed on an actual scraper conveyor, operated under real-life conditions for approx. 18 months.

A number of positive effects of this solution were observed during its operating period. These included the following in particular:

- smooth soft start of the drive system,
- no apparent clutch wear over a period of one and a half years of operation,
- constant chain tension maintained for a long time throughout the period analysed,
- no chain failure cases, despite its significant wear,
- limited wear of the main wheel and the chain itself,
- no significant damage to ejector elements,
- reduced wear on the conveyor housing compared to previous observations.

Once the heading driving was competed, the clutches were dismantled and sent to the manufacturer for further analysis. As part of the assessment, they were disassembled into individual components whose technical condition was examined. Although seals were found to be damaged, no contamination of the lubricant inside the clutch was observed, which demonstrated the effectiveness of its protective structure.

The operation under real-life conditions enabled positive verification of the solution proposed in terms of durability and confirmed the capacity of the device in question to reduce dynamic forces (as evidenced by relatively small damage to the conveyor and no chain failure), however, this still did not make it possible to fully understand the functional – especially vibroacoustic – properties of the flexible clutch designed.

a

b

Fig. 4. The innovative drive unit: a – motor with the flexible clutch, b – gear transmission mounted to the conveyor housing along with the main drive wheel.

The vibroacoustic properties of the innovative clutch have been partially discussed in paper [34], however, what has not been considered in that study is the variation of the load form nearing that of real-life operation, while only the load spikes typical of the scraper blocking situation have been verified. Consequently, the scope of this study and of the load cases analysed is multiple times greater.

In contrast, this paper provides extensive identification of the vibroacoustic properties of the drive system coupled with the innovative flexible clutch. In fact, during operation, one can observe load torque changes of different nature, including short phases of operation under virtually constant load. This is why load torque changes of diverse nature have been discussed and the possibility of reducing the vibration acceleration of drive system components during operation with different loads has been analysed in this paper.

2. Research stand

The research stand was an innovative drive system featuring a dedicated flexible clutch (Fig. 5) designed for mining scraper conveyor drives. This clutch is the main part of the flexible clutch, whose other part, i.e. the insert-type clutch, was not used on account of the high-precision alignment of the drive shafts. Illustrated in Fig. 6 and 7, this system consists of the following elements: an electric driving motor, the innovative torsionally flexible clutch, making it possible to achieve high values of torsion angles owing to its screw gear mechanism, a shaft with cardan joints, an assembly of two multi-stage gear transmissions, of which the first worked as a reducing gear and the second one as a multiplying gear, as well as an electric braking motor

(Fig. 7, item S2). Fig. 7 shows a diagram of the arrangement of measuring points, while Fig. 6 shows the location of the tachometer probe generating the tacho signal.

Fig. 5. Innovative flexible clutch mounted at a test rig (in-house resources).

Fig. 6. Drive system subject to tests with the innovative flexible clutch.

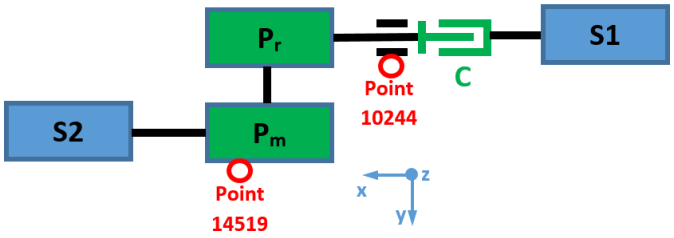

Fig. 7. Diagram of locations of measuring points and other elements: S1 – electric motor, C –flexible clutch, P – toothed gear (gear for reduction rotation velocity – r; gear for multiplication rotation - m), S2 – electric loading motor.

The solution used to reduce the acceleration of the vibrations observed at selected points of the drive system under study was the original torsionally flexible clutch (a part of the flexible damping clutch and an all-metal component), described in detail in section 2 of this paper, in which rotary motion is converted by means of a screw mechanism into progressive motion, thus causing compression of a disc spring pack. This type of clutch can be characterised by a high value of the torsion angle of its members, even as high as above 200°. Fig. 8 shows the non-linear form of the characteristic of the element studied. What this characteristic shows is that the clutch stiffness increases significantly for torque values above approx. 1,125 Nm. Fig. 8 also provides the equations which make it possible to determine the two characteristic ranges; they are marked in blue and orange.

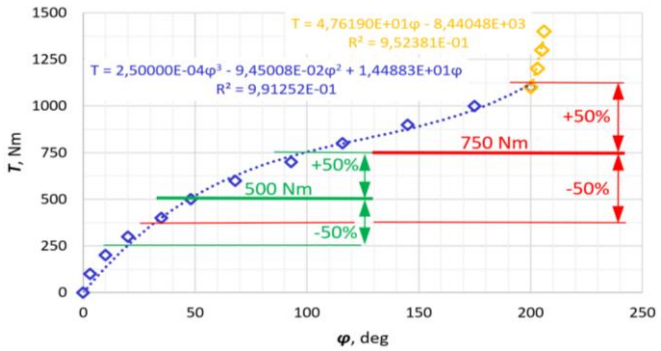

Fig. 8. Characteristic stiffness curve (non-linear form) of the clutch studied (authors' own elaboration).

The analysis comprised both lower loads, where the nominal load value (mean value over a variable cycle) was 500 Nm ±50% of the nominal value, and this range has been marked in green in Fig. 8, as well as higher loads, where the nominal load value (mean value over a variable cycle) was 750 Nm ±50% of the nominal value, and this range has been highlighted in red in Fig. 8. The load values were chosen so as to analyse the clutch operation within the degressive characteristic curve range for lower loads (range marked in green in Fig. 8) as well as within the degressive and progressive characteristic curve range for higher loads (range marked in red in Fig. 8).

On account of the non-linear nature of the clutch operation, in the case of the lower of the loads analysed, a decrease in the load value from the nominal one (500 Nm) by 50% results in a decrease in the torsion angle of the clutch members by as much as ~60% (~50° - ~20° = ~30° – see Fig. 8), while an increase in the load value from the nominal one (500 Nm) by 50% results in an increase in the torsion angle of the clutch members by as much as 100% (~100° - ~50° = ~50° – see Fig. 8). On the other hand, in the case of the higher of the loads analysed, decreasing the load value from the nominal one (750 Nm) by 50% results in a decrease in the torsion angle of the clutch members by as much as ~70% (~100° - ~30° = ~70° – see Fig. 8), while an increase in the load value from the nominal one (750 Nm) by 50% results in an increase in the torsion angle of the clutch members by as much as 100% (~200° - ~100° = ~100° – see

Fig. 8).

In order to analyse the variations in the vibration accelerations observed in the drive system featuring the innovative flexible clutch, the research object was tested under a constant load (designation N) as well as in line with different load torque variation waveforms in a function of time. The waveforms applied were sinusoidal (designation S), rectangular (designation P), and triangular (designation T).

Two nominal load torque values were adopted: 500 Nm and 750 Nm, and in the case of the variable loads, the amplitude of the said waveforms for the braking torque variation was ±50% of the nominal value. The period of the load torque change cycle was chosen on the basis of the authors' previous experiences related to the operation of scraper conveyor drive systems, and so it was set at 6 s, while the rotational speed of the driving motor shaft was typical, fluctuating around approx. 1,480 RPM. The tests were conducted with the clutch in the flexible operating mode (designation P) as well as with the clutch locked (designation L). The foregoing means that 32 different modes of the drive system operation were examined. The vibration acceleration signals chosen for analysis were recorded in all three measurement directions: *x*, *y*, *z* (see Fig. 7) and two relevant measurement points: at the support of the clutch mounted on the system's drive shaft – point no. 10244 located between the driving motor and the reducing gear (Figs. 5–7), and at the multiplying gear housing, at the same time being relatively close to the braking motor – point no. 14519 (Figs. 6 and 7). This means that as many as 192 different time waveforms, recorded over the course of the tests which posed serious technical difficulties, were subject to amplitude, frequency, and time-frequency analyses.

3. Amplitude analysis of recorded signals

Having compared the flexible (Fig. 9b) and rigid (Fig. 9a) modes of the clutch operation, one can clearly notice a significant reduction in the RMS of vibration accelerations from a maximum of 33.9 m/s^2 to 26.1 m/s^2 caused by the rigid operation of the clutch. Furthermore, it is evident that, in the locked operating mode of the clutch, the dominant RMS of vibration accelerations were observed in direction *y* (see Fig. 7), while in the case of the torsional flexible operation – in direction *x*.

Figures 10a and 10b, on the other hand, show the RMS of the vibration acceleration signal measured at point 14519 (see Fig. 7) for the same load values and waveforms. Analysis of the results depicted in Figure 10 implies that no significant reductions in vibration accelerations were recorded at this point, except for the constant load (N) – in all directions: *x*, *y*, *z*, as well as for the triangular waveform load (T) – in directions *x* and *y*. However, it should be noted that the RMS of vibration accelerations measured at point 14519 in the locked clutch operating mode were up to five times lower than those obtained at point 10244. This makes the above-described considerable reduction of vibration accelerations at point 10244 relevant, since that is where the vibration acceleration were initially higher, only to be significantly reduced (Fig. 9).

a)

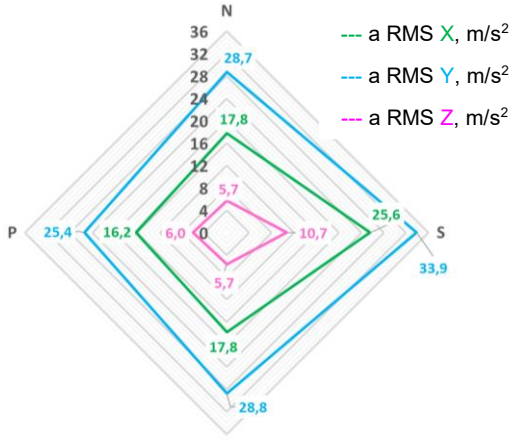

b)

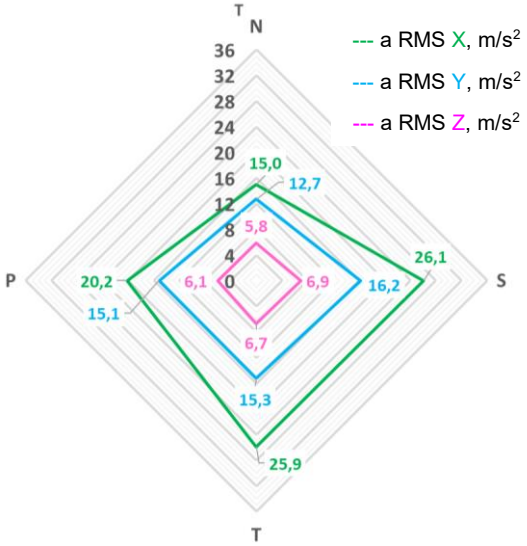

Fig. 9. RMS of the vibration acceleration signal measured at point 10244 in three directions: *x*, *y*, *z*, with the system subject to load torque: constant of 500 Nm (designation N), with sinusoidally variable waveform (designation S), with triangular waveform (designation T), and with rectangular waveform (designation P), 500 ±250 Nm: a) clutch operating in the locked mode, b) clutch operating in the flexible mode.

a)

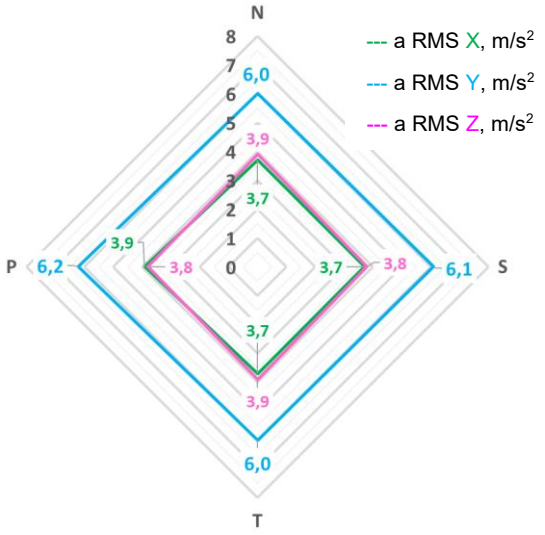

b)

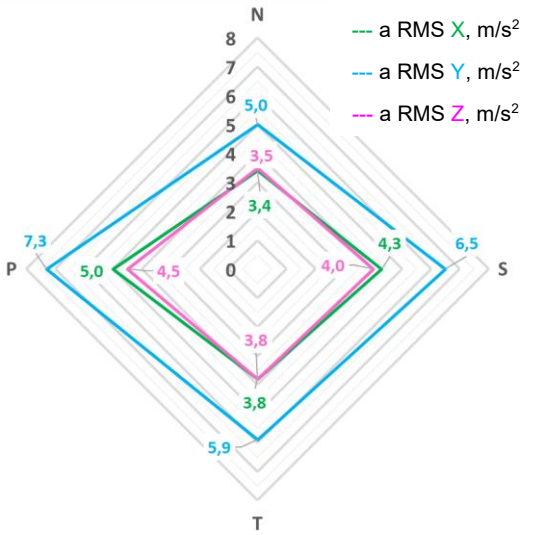

Fig. 10. RMS of the vibration acceleration signal measured at point 14519 in three directions: *x*, *y*, *z*, with the system subject to load torque: constant of 500 Nm (designation N), with sinusoidally variable waveform (designation S), with triangular waveform (designation T), and with rectangular waveform (designation P), 500 ±250 Nm: a) clutch operating in the locked mode, b) clutch operating in the flexible mode.

In the case of the higher load with the constant value of 750 Nm and with the variable value of 750 ±375 Nm, having compared the RMS of the vibration accelerations observed with the clutch in the rigid operating mode (Fig. 11a) and those established in the flexible operating mode (Fig. 11b), one can observe a significant reduction in the RMS of vibration accelerations from a maximum of 38.5 m/s^2 to 21.2 m/s^2 caused by the flexible clutch operation. As in the case of the smaller time-varying loads (500 ±250 Nm), so in the locked operating mode of the clutch, it can be noticed that the dominant RMS of vibration accelerations were observed in direction *y* (see Fig. 7), while in the case of the torsional flexible operation – in direction *x*.

a)

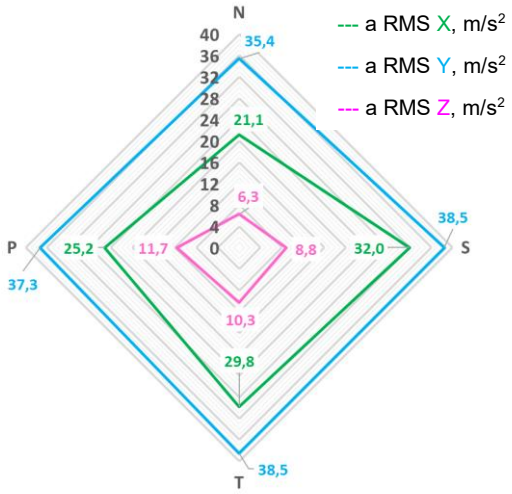

b)

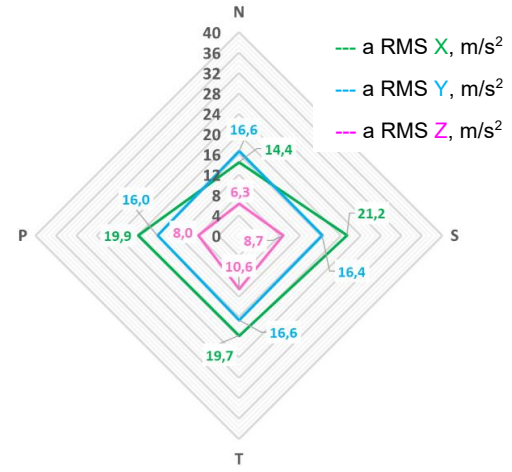

Fig. 11. RMS of the vibration acceleration signal measured at point 10244 in three directions: *x*, *y*, *z*, with the system subject to load torque: constant of 750 Nm (designation N), with sinusoidally variable waveform (designation S), with triangular waveform (designation T), and with rectangular waveform (designation P), 750 ±375 Nm: a) clutch operating in the locked mode, b) clutch operating in the flexible mode.

Figures 12a and 12b, on the other hand, show the RMS of the vibration acceleration signal measured at point 14519 for the following loads: constant of 750 Nm and variable of 750±375 Nm. Analysis of the results shown in Figure 10 further implies that no significant change in vibration accelerations was recorded at this point, and therefore, in this case as well, the reduction in the RMS of the vibration accelerations measured at the higher load at point 10244, where the values were reduced significantly from a much higher level, becomes relevant.

The differences observed with a given measurement parameter (i.e. given a certain load torque and certain loading

nature, and at a given measurement point in a given measurement direction) between the RMS of the vibration accelerations measured with the clutch operating in the flexible mode and the RMS of the vibration accelerations measured with the clutch operating in the locked mode were analysed against the maximum RMS of the vibration accelerations recorded when one of the two nominal loads were applied and with the clutch operating in the locked mode with regard to the following: the given nature of the system load variation taken into consideration (N, S, T, P), the given measurement point taken into consideration, and the given measurement direction taken into consideration, and they have been provided in percentage values in Figures 13, 14, and 15. The values described as AVE in the respective of the three figures are average values calculated from the values designated as N, S, T, P in this figure. In the absence of knowledge of the loads of what nature (N, S, T, P) may dominate the system during operation, this value can represent the average RMS decrease/increase potential at a given measurement point, in a given measurement direction, and with a given nominal load.

With reference to the results illustrated in:

- Figure 13 (direction *x*), it can be concluded that the largest average percentage increase in the RMS of vibration accelerations was 7.8% (Fig. 13a), and the largest average reduction thereof was multiple times greater, being as high as 30.1% (Fig. 13c);
- Figure 14, it can be concluded that the largest average percentage increase in the RMS of vibration accelerations for measurement direction *y*, where the largest vibration accelerations occurred, was 0.2% (Fig. 14b), while the largest average decrease thereof was significantly greater, being as much as 56.1% (Fig. 14c);
- Figure 15 (direction *z*), it can be concluded that the largest average percentage increase in the RMS of vibration accelerations was 3.3% (Figure 15d), and the largest average reduction thereof was more than twice as great and amounted to 7.4% (Figure 15c).

a)

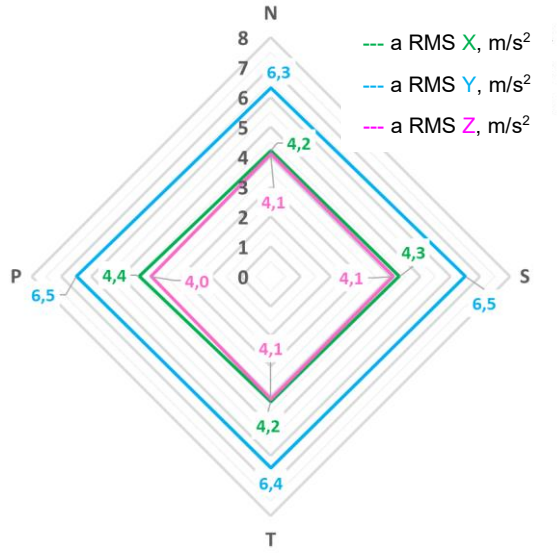

b)

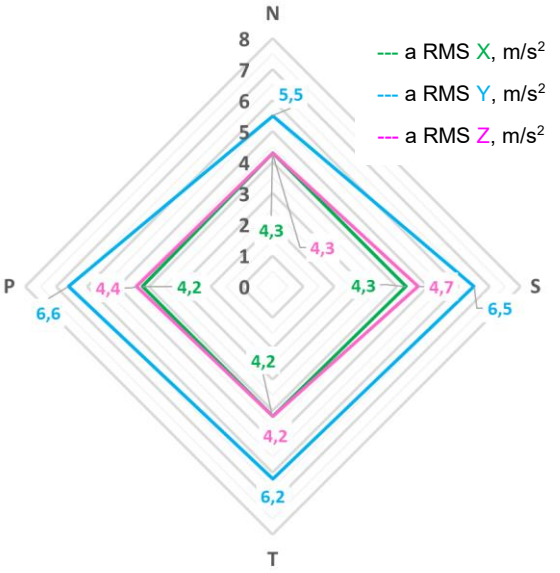

Fig. 12. RMS of the vibration acceleration signal measured at point 14519 in three directions: *x*, *y*, *z*, with the system subject to load torque: constant of 750 Nm (designation N), with sinusoidally variable waveform (designation S), with triangular waveform (designation T), and with rectangular waveform (designation P), 750 ±375 Nm: a) clutch operating in the locked mode, b) clutch operating in the flexible mode.

a)

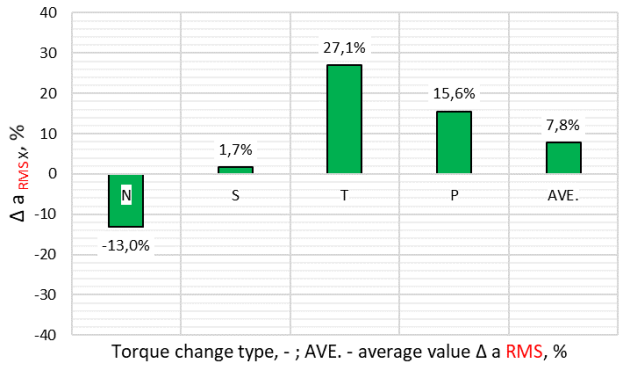

b)

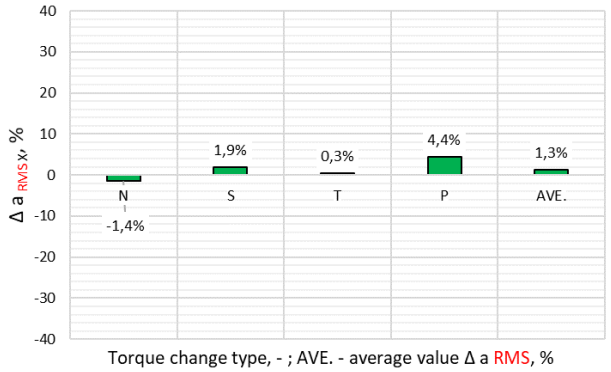

c)

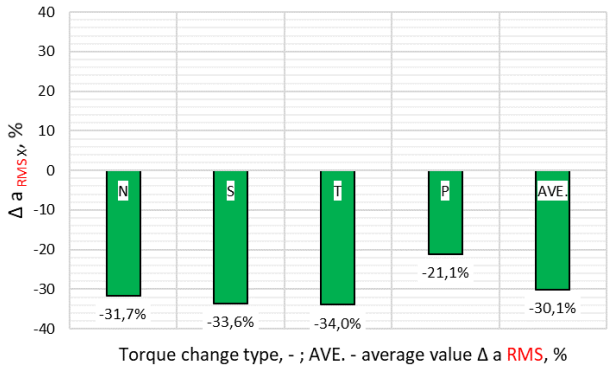

d)

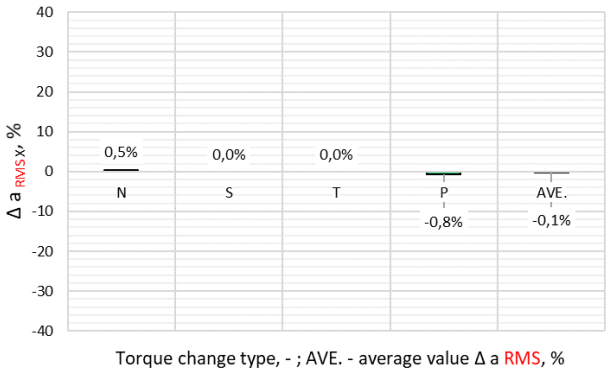

Fig. 13. Changes in the RMS of the vibration acceleration signal recorded in direction *x*, expressed in percents:
a) constant load torque of 500 Nm (N) or variable load torque of 500 ±250 Nm (S, T, P) at measurement point 10244,
b) constant load torque of 500 Nm (N) or variable load torque of 500 ±250 Nm (S, T, P) at measurement point 14519,
c) constant load torque of 750 Nm (N) or variable load torque of 750 ±375 Nm (S, T, P) at measurement point 10244,
d) constant load torque of 750 Nm (N) or variable load torque of 750 ±375 Nm (S, T, P) at measurement point 14519.

a)

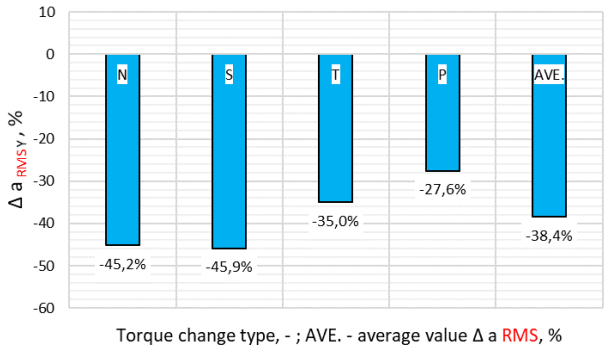

b)

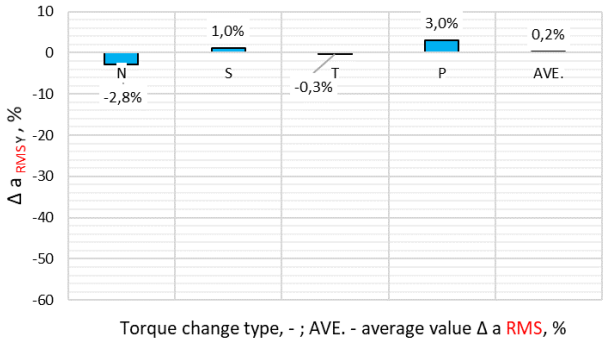

c)

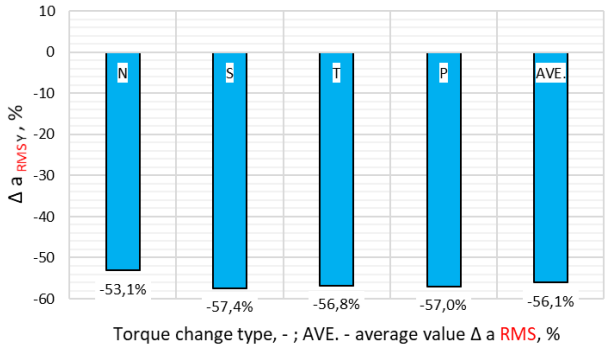

d)

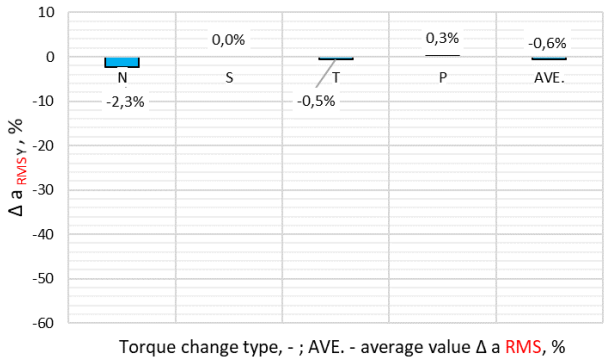

Fig. 14. Changes in the RMS of the vibration acceleration signal recorded in direction *y*, expressed in percents:
a) constant load torque of 500 Nm (N) or variable load torque of 500 ±250 Nm (S, T, P) at measurement point 10244,
b) constant load torque of 500 Nm (N) or variable load torque of 500 ±250 Nm (S, T, P) at measurement point 14519,
c) constant load torque of 750 Nm (N) or variable load torque of 750 ±375 Nm (S, T, P) at measurement point 10244,
d) constant load torque of 750 Nm (N) or variable load torque of 750 ±375 Nm (S, T, P) at measurement point 14519.

Fig. 15. Changes in the RMS of the vibration acceleration signal recorded in direction *z*, expressed in percents: a) constant load torque of 500 Nm (N) or variable load torque of 500 ±250 Nm (S, T, P) at measurement point 10244, b) constant load torque of 500 Nm (N) or variable load torque of 500 ±250 Nm (S, T, P) at measurement point 14519, c) constant load torque of 750 Nm (N) or variable load torque of 750 ±375 Nm (S, T, P) at measurement point 10244, d) constant load torque of 750 Nm (N) or variable load torque of 750 ±375 Nm (S, T, P) at measurement point 14519.

Another stage in the studies was an analysis of the peak-to-peak (P-P) shown in Figures 16–19. Having compared the flexible (Fig. 16b) and rigid (Fig. 16a) modes of the clutch operation, one can clearly notice a significant reduction in the peak-to-peak of vibration accelerations from a maximum of 273.8 m/s^2 to 171.9 m/s^2 caused by the rigid operation of the clutch. Furthermore, it is evident that, in the locked operating mode of the clutch, the dominant RMS of vibration accelerations were observed in direction *y* (see Fig. 7), while in the case of the torsional flexible operation – in direction *x*.

Figures 17a and 17b, on the other hand, show the peak-to-peak (P-P) of the linear vibration acceleration signal measured at point 14519 (Fig. 14519) for the same load values and waveforms. Analysis of the results depicted in Figure 17 implies that no significant reductions in vibration accelerations were recorded at this point, except for the constant load (N) – in directions *x* and *z*. However, it should also be noted that the RMS of vibration accelerations measured at point 14519 in the locked clutch operating mode were approximately five times lower than those obtained at point 10244, and so in the case of the peak-to-peak as well, that makes the above-described considerable reduction of vibration accelerations at point 10244 relevant, since that is where the peak-to-peak vibration acceleration were initially higher, only to be significantly reduced (Fig. 16).

a)

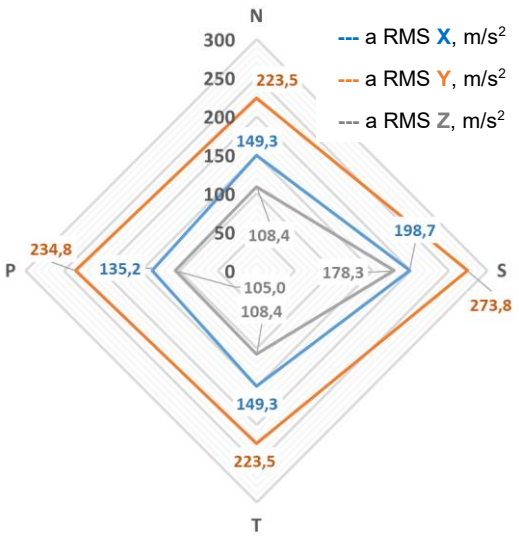

b)

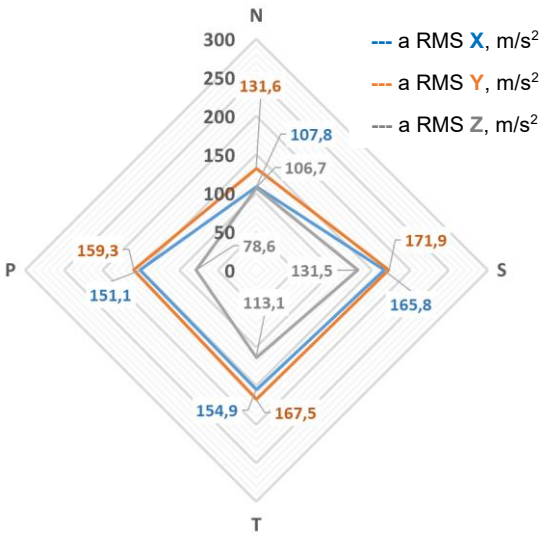

Fig. 16. Peak-to-peak (P-P) of the vibration acceleration signal measured at point 10244 in three directions *x*, *y, z*, with the system subject to load torque: constant of 500 Nm (designation N), with sinusoidally variable waveform (designation S), with triangular waveform (designation T), and with rectangular waveform (designation P), 500 ±250 Nm: a) clutch operating in the locked mode, b) clutch operating in the flexible mode.

In the case of the higher load with the constant value of 750 Nm and with the variable value of 750 ±375 Nm, having compared the peak-to-peak of the vibration accelerations observed with the clutch in the rigid operating mode (Fig. 18a) and in the flexible operating mode (Fig. 18b), and at measurement point 10244, one can observe a significant reduction in the peak-to-peak of vibration accelerations from a maximum of 332.9 m/s^2 to 245.6 m/s^2 caused by the flexible clutch operation. It is further evident that, in the locked operating mode of the clutch, the dominant RMS of vibration accelerations were observed in direction *y* (see Fig. 7), while in the case of the torsional flexible operation – in direction *z*.

a)

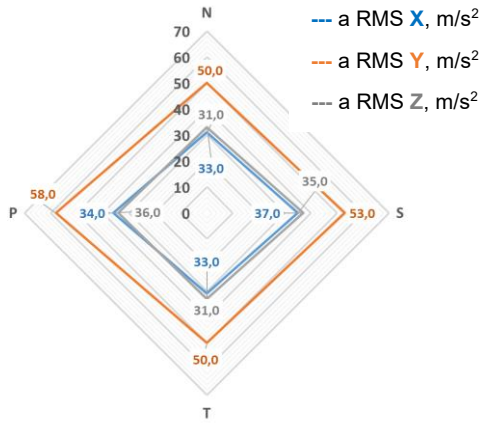

b)

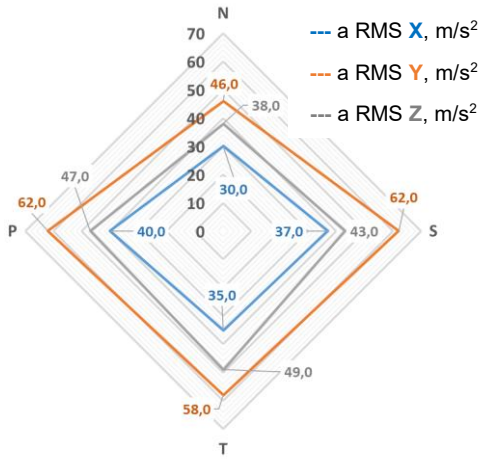

Fig. 17. Peak-to-peak (P-P) of the vibration acceleration signal measured at point 14519 in three directions *x*, *y*, *z*, with the system subject to load torque: constant of 500 Nm (designation N), with sinusoidally variable waveform (designation S), with triangular waveform (designation T), and with rectangular waveform (designation P), 500 ±250 Nm: a) clutch operating in the locked mode, b) clutch operating in the flexible mode.

Figures 19a and 19b, on the other hand, show the peak-to-peak of the vibration acceleration signal measured at point 14519 for the following loads: constant of 750 Nm and variable of 750 ±375 Nm. Analysis of the results illustrated in these figures implies that no significant change in vibration accelerations was recorded at this point (compared to the variations measured at point 10244), and therefore, in this case as well, the reduction in the RMS of the vibration accelerations measured at point 10244, where the values were reduced significantly from a much higher level, becomes relevant.

Figures 20, 21, and 22 show the relevant peak-to-peak (P-P) values, calculated similarly to the RMS and expressed in percents alike. The values described as AVE in the respective of the three figures are average values calculated from the values designated as N, S, T, P in this figure. In the absence of knowledge of the loads of what nature (N, S, T, P) may dominate the system during operation, this value can represent the average peak-to-peak (P-P) reduction/increase potential at a given measurement point, in a given measurement direction, and with a given nominal load.

a)

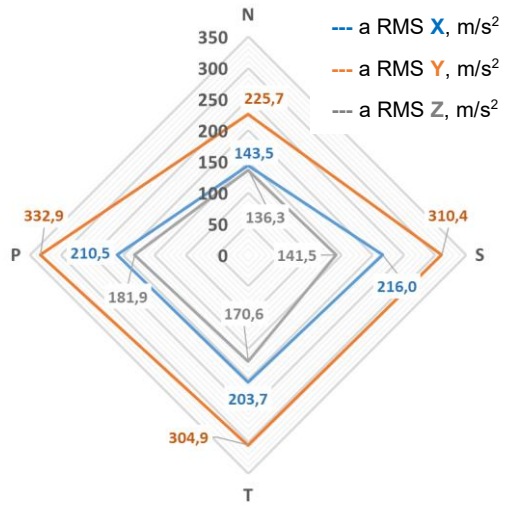

b)

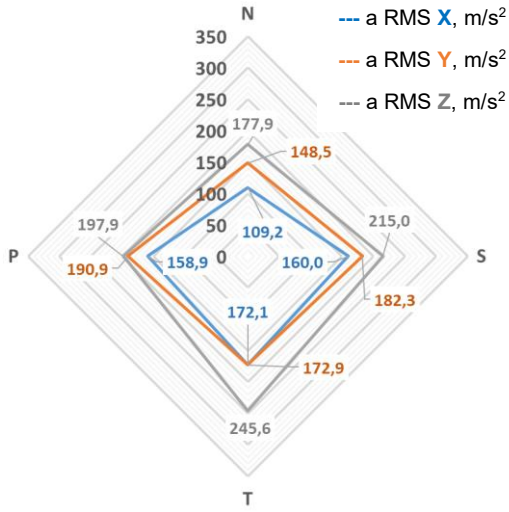

Fig. 18. Peak-to-peak (P-P) of the vibration acceleration signal measured at point 10244 in three directions *x*, *y*, *z*, with the system subject to load torque: constant of 750 Nm (designation N), with sinusoidally variable waveform (designation S), with triangular waveform (designation T), and with rectangular waveform (designation P), 750 ±375 Nm: a) clutch operating in the locked mode, b) clutch operating in the flexible mode.

With reference to the results illustrated in:

- Figure 20 (direction *x*), it can be concluded that the largest average percentage increase in the peak-to-peak (P-P) of vibration accelerations was 1% (Fig. 20b), and the largest average reduction thereof was more than twenty times greater, being as high as 22.2% (Fig. 10c);
- Figure 21, it can be concluded that the largest average percentage increase in the peak-to-peak (P-P) of vibration accelerations for measurement direction *y*, where the largest vibration accelerations occurred, was 1.2% (Fig. 21b), while the largest average decrease thereof was several dozen times greater, being as much as 40.4% (Fig. 21c);
- Figure 22 (direction *z*), it can be concluded that the largest average percentage increase in the peak-to-peak (P-P) of vibration accelerations was 31.1% (Figure 22c), and the largest average reduction thereof was smaller only in this particular case, as it came to 9.8% (Figure 22a).

a)

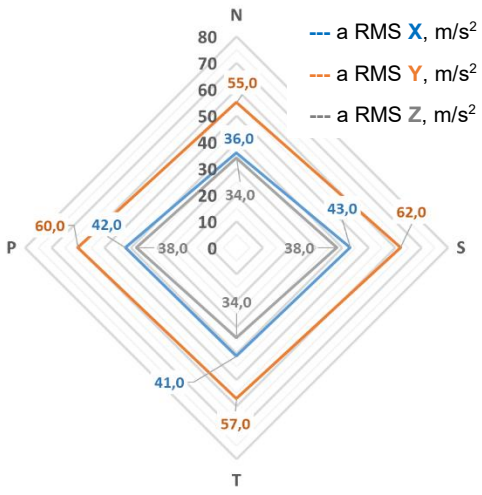

b)

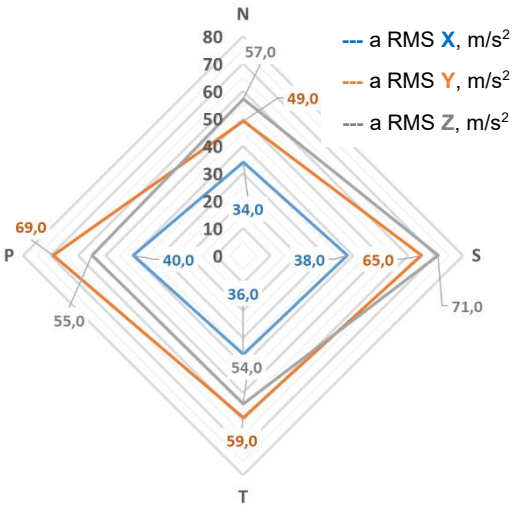

Fig. 19. Peak-to-peak (P-P) of the vibration acceleration signal measured at point 14519 in three directions *x*, *y*, *z*, with the system subject to load torque: constant of 750 Nm (designation N), with sinusoidally variable waveform (designation S), with triangular waveform (designation T), and with rectangular waveform (designation P), 750 ±375 Nm: a) clutch operating in the locked mode, b) clutch operating in the flexible mode.

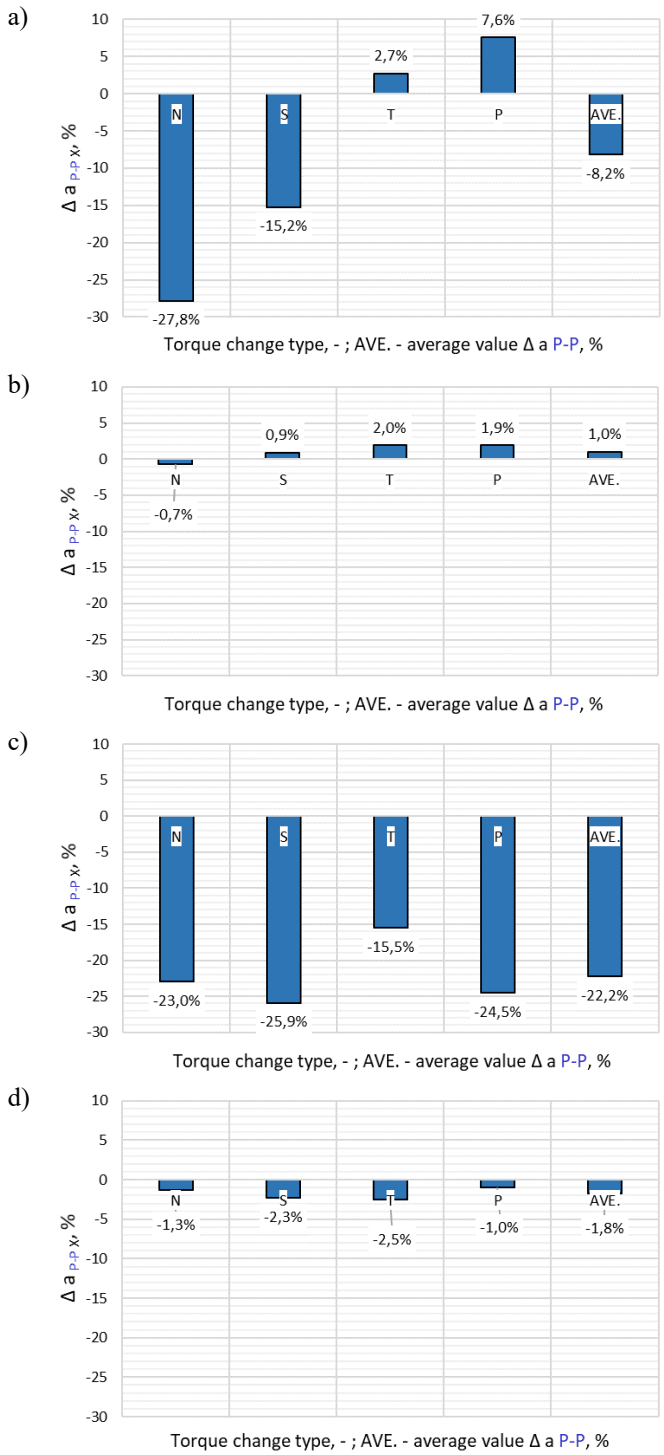

Fig. 20. Changes in the peak-to-peak (P-P) of the vibration acceleration signal recorded in direction *x*, expressed in percents: a) constant load torque of 500 Nm (N) or variable load torque of 500 ±250 Nm (S, T, P) at measurement point 10244, b) constant load torque of 500 Nm (N) or variable load torque of 500 ±250 Nm (S, T, P) at measurement point 14519, c) constant load torque of 750 Nm (N) or variable load torque of 750 ±375 Nm (S, T, P) at measurement point 10244, d) constant load torque of 750 Nm (N) or variable load torque of 750 ±375 Nm (S, T, P) at measurement point 14519.

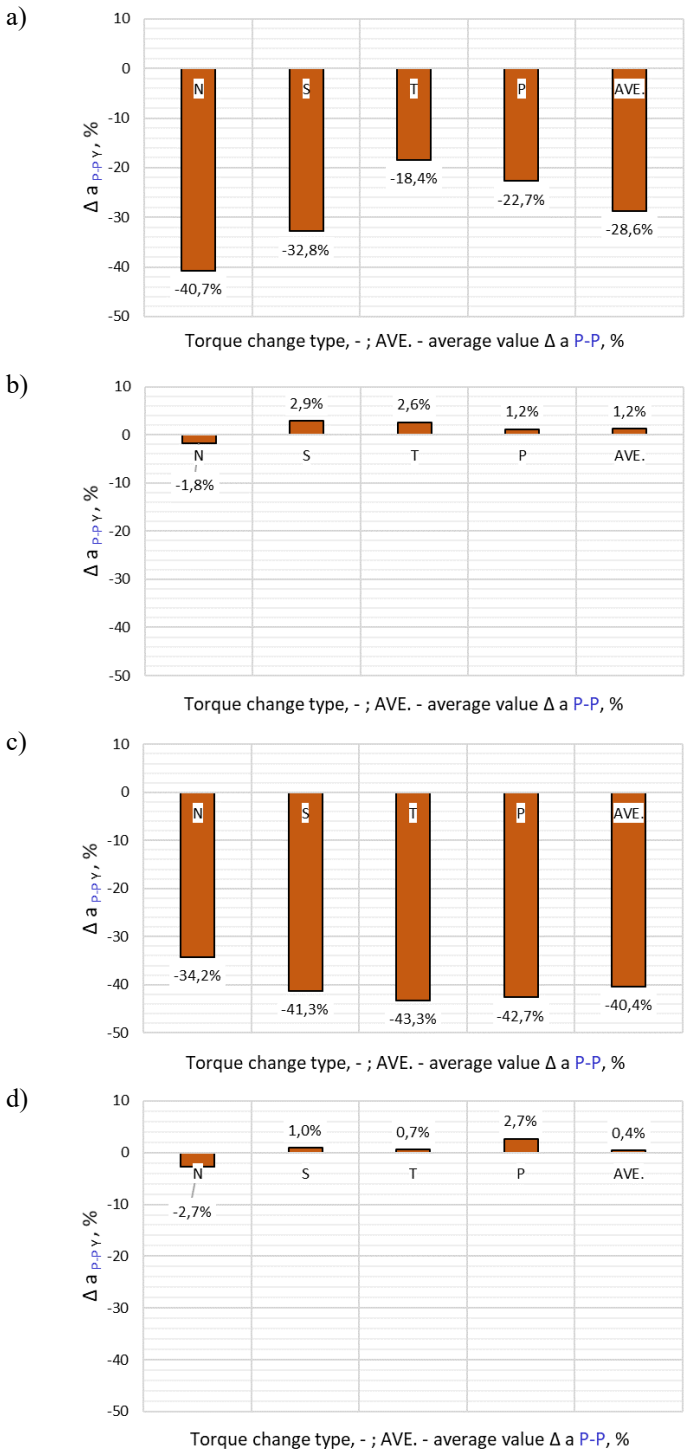

Fig. 21. Changes in the peak-to-peak (P-P) of the vibration acceleration signal recorded in direction *y*, expressed in percents: a) constant load torque of 500 Nm (N) or variable load torque of 500 ±250 Nm (S, T, P) at measurement point 10244, b) constant load torque of 500 Nm (N) or variable load torque of 500 ±250 Nm (S, T, P) at measurement point 14519, c) constant load torque of 750 Nm (N) or variable load torque of 750 ±375 Nm (S, T, P) at measurement point 10244, d) constant load torque of 750 Nm (N) or variable load torque of 750 ±375 Nm (S, T, P) at measurement point 14519.

a)

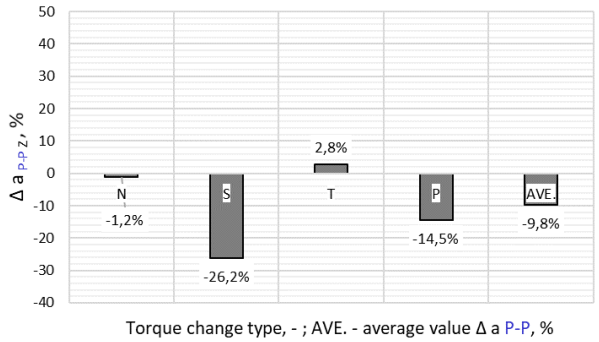

b)

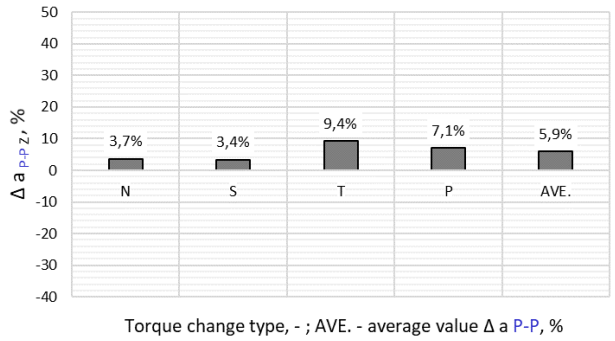

c)

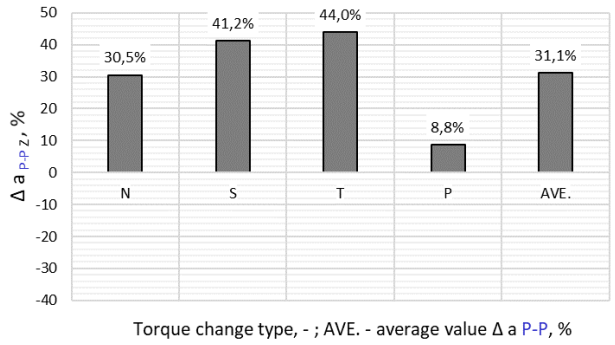

d)

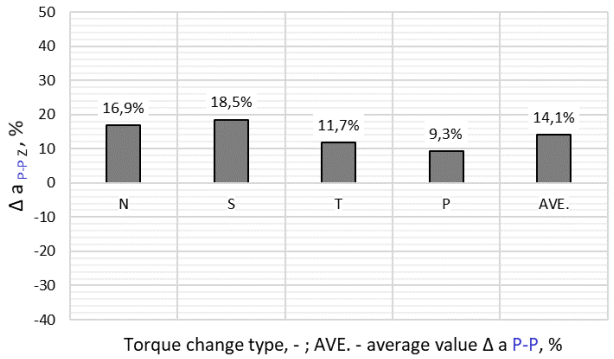

Fig. 22. Changes in the peak-to-peak (P-P) of the vibration acceleration signal recorded in direction *z*, expressed in percents: a) constant load torque of 500 Nm (N) or variable load torque of 500 ±250 Nm (S, T, P) at measurement point 10244, b) constant load torque of 500 Nm (N) or variable load torque of 500 ±250 Nm (S, T, P) at measurement point 14519, c) constant load torque of 750 Nm (N) or variable load torque of 750 ±375 Nm (S, T, P) at measurement point 10244, d) constant load torque of 750 Nm (N) or variable load torque of 750 ±375 Nm (S, T, P) at measurement point 14519.

Figure 23 provides a compilation of the average percentage changes in the RMS and peak-to-peak (P-P) of the vibration acceleration signal recorded in different directions and at different measurement points. The yellow colour represents the average values obtained for both measurement points analysed. The highest of the reductions of the RMS vibration acceleration values thus calculated is 23.7%, while for the peak-to-peak (P-P) vibration acceleration values, it is 16.8%.

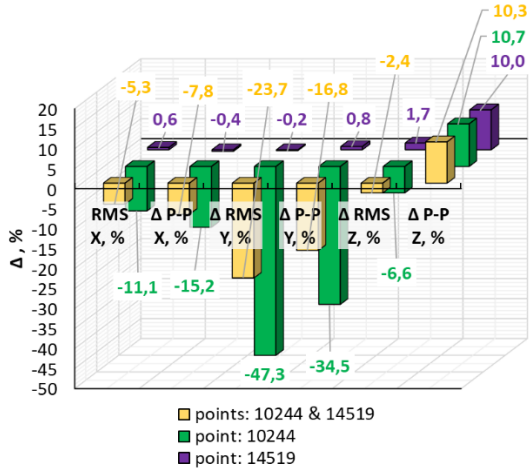

Fig. 23. Compilation of the average percentage changes in the RMS and peak-to-peak (P-P) of the vibration acceleration signal recorded in different directions and at different measurement points.

4. Frequency-amplitude and time-frequency analysis

The studies addressed in this paper also included a frequency analysis of the vibration signals recorded. Figure 24b shows the values of the maximum amplitudes observed in the frequency spectrum for the vibration acceleration signals measured at point 10244, while Figure 24a shows the frequencies corresponding to the said maximum values. Additionally, Figure 24a also implies that, for measurement direction *y*, the frequency corresponding to the maximum amplitude value was in a relatively narrow range from 1,364 Hz to 1,469 Hz. This was not the case of the other measurement directions.

A conclusion which can be drawn from Figure 24b is that, for direction *y*, given the relevant changes in the braking torque values and the nature of the load torque changes (N, S, T, P), the maximum amplitude found in the frequency spectrum always decreased as a result of the clutch operating in the flexible mode (designation P at the end of the markings used in Figures 24–27).

a)

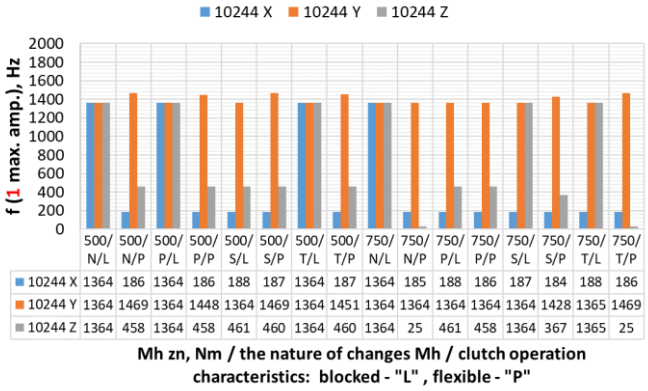

	500/ N/L	500/ N/P	500/ P/L	500/ P/P	500/ S/L	500/ S/P	500/ T/L	500/ T/P	750/ N/L	750/ N/P	750/ P/L	750/ P/P	750/ S/L	750/ S/P	750/ T/L	750/ T/P
10244 X	1364	186	1364	186	188	187	1364	187	1364	185	188	186	187	184	188	186
10244 Y	1364	1469	1364	1448	1364	1469	1364	1451	1364	1364	1364	1364	1364	1428	1365	1469
10244 Z	1364	458	1364	458	461	460	1364	460	1364	25	461	458	1364	367	1365	25

b)

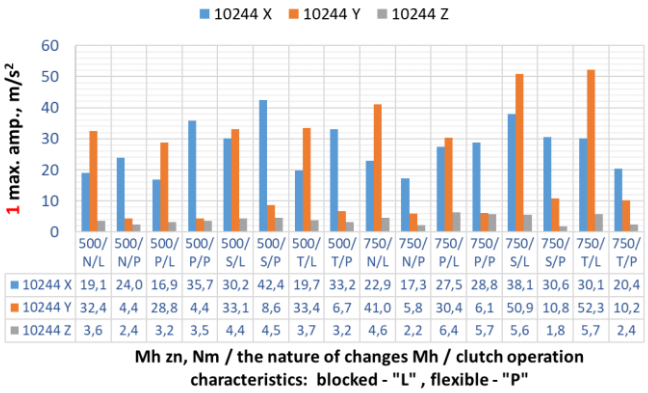

	500/ N/L	500/ N/P	500/ P/L	500/ P/P	500/ S/L	500/ S/P	500/ T/L	500/ T/P	750/ N/L	750/ N/P	750/ P/L	750/ P/P	750/ S/L	750/ S/P	750/ T/L	750/ T/P
10244 X	19,1	24,0	16,9	35,7	30,2	42,4	19,7	33,2	22,9	17,3	27,5	28,8	38,1	30,6	30,1	20,4
10244 Y	32,4	4,4	28,8	4,4	33,1	8,6	33,4	6,7	41,0	5,8	30,4	6,1	50,9	10,8	52,3	10,2
10244 Z	3,6	2,4	3,2	3,5	4,4	4,5	3,7	3,2	4,6	2,2	6,4	5,7	5,6	1,8	5,7	2,4

Fig. 24. Compilation of values, measurement point 10244: a) frequencies corresponding to the maximum amplitude observed in the frequency spectrum, b) maximum amplitude values recorded in the frequency spectrum.

The same outcome was obtained when analysing the second maximum amplitude observed within the frequency spectrum (Figure 25b). At this point, it should be reminded that measurement direction *y* was the one in which the RMS of the vibration accelerations prevailed in the case of the locked clutch operation at both measurement points and with all the characteristics of the load torque variations (Figs. 9a, 10a, 11a, 12a). The frequency values corresponding to these two aforementioned maxima have been collated in Figures 24a and 25a, rounded off to natural numbers. What can be concluded with reference to these figures is that, apart from one exception out of 32 cases analysed, the frequency values did not change significantly as a result of the flexible clutch operation (with the exception of the case marked as 750/T/P – Figure 25a).

a)

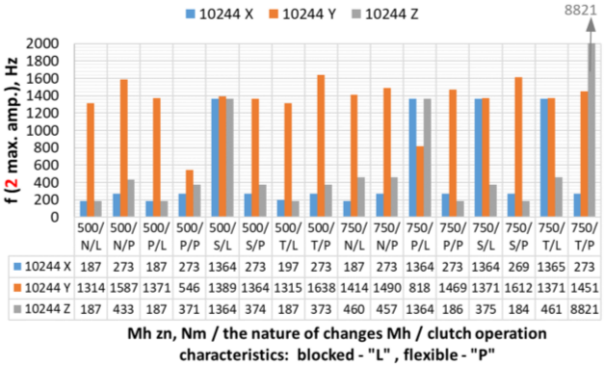

	500/ N/L	500/ N/P	500/ P/L	500/ P/P	500/ S/L	500/ S/P	500/ T/L	500/ T/P	750/ N/L	750/ N/P	750/ P/L	750/ P/P	750/ S/L	750/ S/P	750/ T/L	750/ T/P
10244 X	187	273	187	273	1364	273	197	273	187	273	1364	273	1364	269	1365	273
10244 Y	1314	1587	1371	546	1389	1364	1315	1638	1414	1490	818	1469	1371	1612	1371	1451
10244 Z	187	433	187	371	1364	374	187	373	460	457	1364	186	375	184	461	8821

b)

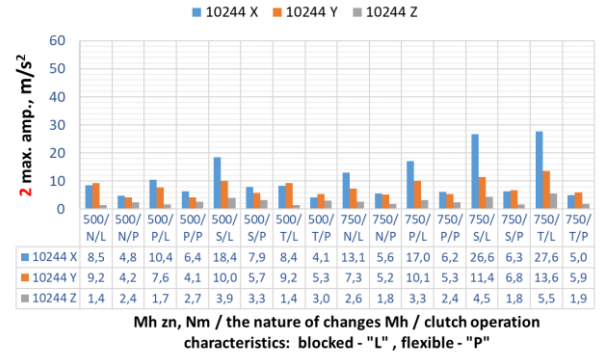

	500/ N/L	500/ N/P	500/ P/L	500/ P/P	500/ S/L	500/ S/P	500/ T/L	500/ T/P	750/ N/L	750/ N/P	750/ P/L	750/ P/P	750/ S/L	750/ S/P	750/ T/L	750/ T/P
10244 X	8,5	4,8	10,4	6,4	18,4	7,9	8,4	4,1	13,1	5,6	17,0	6,2	26,6	6,3	27,6	5,0
10244 Y	9,2	4,2	7,6	4,1	10,0	5,7	9,2	5,3	7,3	5,2	10,1	5,3	11,4	6,8	13,6	5,9
10244 Z	1,4	2,4	1,7	2,7	3,9	3,3	1,4	3,0	2,6	1,8	3,3	2,4	4,5	1,8	5,5	1,9

Fig. 25. Compilation of values recorded at measurement point 10244: a) frequencies corresponding to the second maximum amplitude observed in the frequency spectrum, b) second maximum amplitude recorded in the frequency spectrum.

As already shown in Figure 24a, it can be observed that, in the case of measurement direction *y*, the frequency corresponding to the maximum amplitude value was contained in a relatively narrow range from 1,364 Hz to 1,469 Hz. This was neither the case for measurement point 14519 (Fig. 26a), nor for the other measurement directions (Fig. 26a). On the other hand, for point 14519 and direction *y*, the maximum amplitude observed in the frequency spectrum was often found not to decline as a result of the clutch operating in the flexible mode (Fig. 26b).

a)

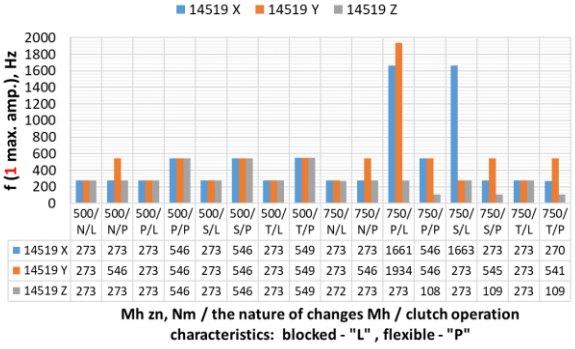

	500/ N/L	500/ N/P	500/ P/L	500/ P/P	500/ S/L	500/ S/P	500/ T/L	500/ T/P	750/ N/L	750/ N/P	750/ P/L	750/ P/P	750/ S/L	750/ S/P	750/ T/L	750/ T/P
14519 X	273	273	273	546	273	546	273	549	273	273	1661	546	1663	273	273	270
14519 Y	273	546	273	546	273	546	273	549	273	546	1934	546	273	545	273	541
14519 Z	273	273	273	546	273	546	273	549	272	273	273	108	273	109	273	109

b)

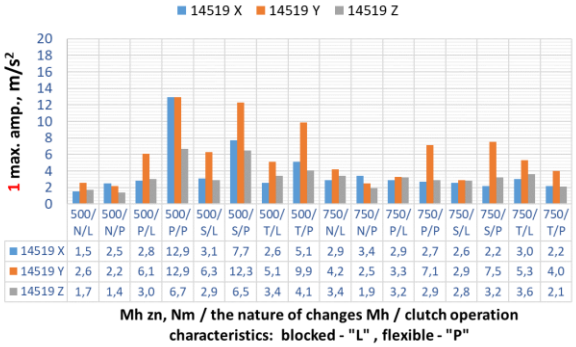

	500/ N/L	500/ N/P	500/ P/L	500/ P/P	500/ S/L	500/ S/P	500/ T/L	500/ T/P	750/ N/L	750/ N/P	750/ P/L	750/ P/P	750/ S/L	750/ S/P	750/ T/L	750/ T/P
14519 X	1,5	2,5	2,8	12,9	3,1	7,7	2,6	5,1	2,9	3,4	2,9	2,7	2,6	2,2	3,0	2,2
14519 Y	2,6	2,2	6,1	12,9	6,3	12,3	5,1	9,9	4,2	2,5	3,3	7,1	2,9	7,5	5,3	4,0
14519 Z	1,7	1,4	3,0	6,7	2,9	6,5	3,4	4,1	3,4	1,9	3,2	2,9	2,8	3,2	3,6	2,1

Fig. 26. Compilation of values, measurement point 14519: a) frequencies corresponding to the maximum amplitude observed in the frequency spectrum, b) maximum amplitude recorded in the frequency spectrum.

The same outcome was obtained when analysing the second maximum amplitude observed within the frequency spectrum (Figure 27b). However, it is noteworthy that, at point 10244, where the vibration acceleration values in the locked clutch operation case were approximately five times greater than at point 14519, a reduction in the vibration amplitudes was observed (compare Fig. 9a, 10a, 11a, 2a). Nevertheless, due to the greater mass concentrated around point 14519 than around point 10244, the frequencies measured at point 14519 and corresponding to the maximum values were lower than those obtained at point 10244 in the decided majority of the cases analysed (compare Fig. 24a with 26a). Frequencies corresponding to the second maximum amplitude observed in the frequency spectrum in the case of measurement point 14519 change in a fairly wide range, exceeding 400 Hz (Fig. 27a).

a)

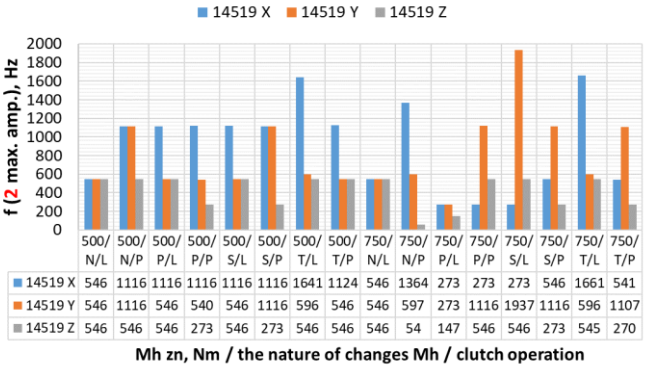

	500/ N/L	500/ N/P	500/ P/L	500/ P/P	500/ S/L	500/ S/P	500/ T/L	500/ T/P	750/ N/L	750/ N/P	750/ P/L	750/ P/P	750/ S/L	750/ S/P	750/ T/L	750/ T/P
14519 X	546	1116	1116	1116	1116	1116	1641	1124	546	1364	273	273	273	546	1661	541
14519 Y	546	1116	546	540	546	1116	596	546	546	597	273	1116	1937	1116	596	1107
14519 Z	546	546	546	273	546	273	546	546	546	54	147	546	546	273	545	270

b)

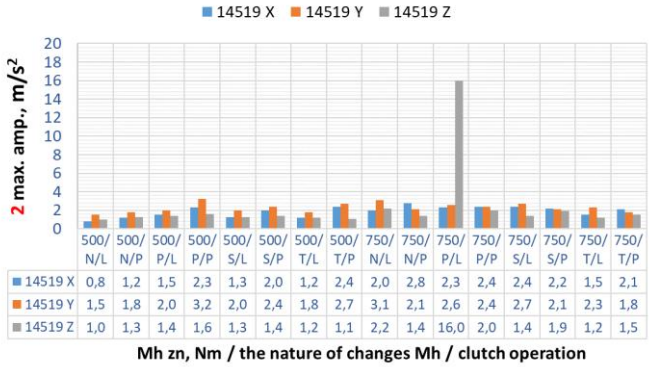

	500/ N/L	500/ N/P	500/ P/L	500/ P/P	500/ S/L	500/ S/P	500/ T/L	500/ T/P	750/ N/L	750/ N/P	750/ P/L	750/ P/P	750/ S/L	750/ S/P	750/ T/L	750/ T/P
14519 X	0,8	1,2	1,5	2,3	1,3	2,0	1,2	2,4	2,0	2,8	2,3	2,4	2,4	2,2	1,5	2,1
14519 Y	1,5	1,8	2,0	3,2	2,0	2,4	1,8	2,7	3,1	2,1	2,6	2,4	2,7	2,1	2,3	1,8
14519 Z	1,0	1,3	1,4	1,6	1,3	1,4	1,2	1,1	2,2	1,4	16,0	2,0	1,4	1,9	1,2	1,5

Fig. 27. Compilation of values, measurement point 14519: a) frequencies corresponding to the second maximum amplitude observed in the frequency spectrum, b) second maximum amplitude values recorded in the frequency spectrum.

Time-frequency analysis makes it possible to observe effects that are unobservable over the course of amplitude or frequency analysis. With regard to the foregoing, Figure 28 shows the STFT time-frequency distributions obtained on the basis of the signals recorded:

- at measurement point 10244,
- in the relevant *y* direction,
- for a load of 500 ±250 Nm and the triangular waveform of its variations,

as well as for the clutch operating in both the locked (Fig. 28a) and the flexible mode (Fig. 28b). It is evident that, on account of the torsional flexible operation of the clutch, in this case, there was a considerable (nearly threefold) reduction in the maximum values of the STFT spectrum amplitudes depicted on the time-frequency plane (see *colour bars* in Fig. 28).

a)

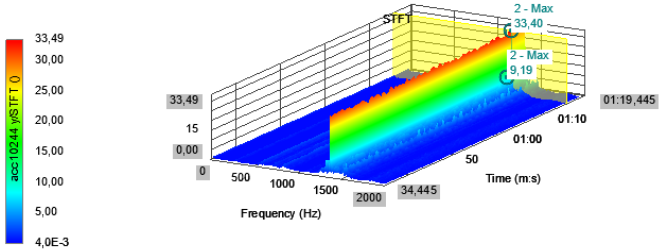

b)

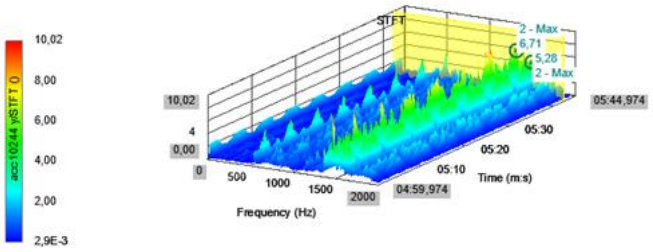

Fig. 28. STFT time-frequency analysis of the signals, measurement point 10244 in direction *y* for a load of 500 ±250 Nm and its triangular waveform (T): a) for clutch in locked operating mode, b) for clutch in flexible operating mode.

With regard to the load variations of other nature at point 10244, a comparable effect was also observed, e.g. as shown in Figure 29. Moreover, in the case of the locked operating mode, this figure (Fig. 29a) clearly shows the effects caused by the sinusoidal torque variation, which are not observed when the clutch operates in the flexible mode in a time-frequency distribution, and there was a significant (nearly fivefold) reduction in the maximum values of the amplitudes recorded in the time-frequency plane (see *colour bars* in Fig. 29).

a)

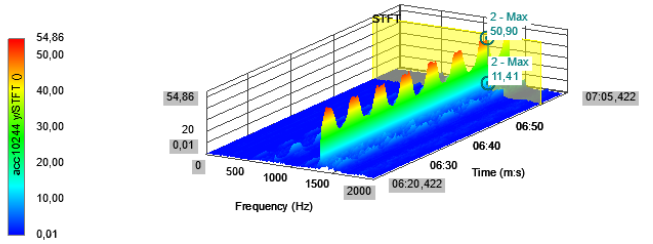

b)

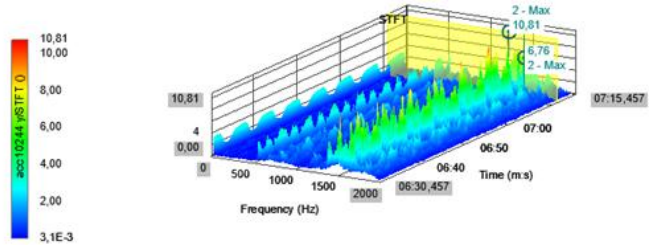

Fig. 29. STFT time-frequency analysis of the signals, measurement point 10244 in direction *y* for a load of 750 ±375 Nm and its sinusoidal waveform (S): a) for clutch in locked operating mode, b) for clutch in flexible operating mode.

The aforementioned effect attributable to the reduction of the maximum amplitudes in the time-frequency plane (see *colour bars* in Fig. 30) is also observable in the case of measurement point 14519, the relevant *y* direction, and even the constant load of 750 Nm.

a)

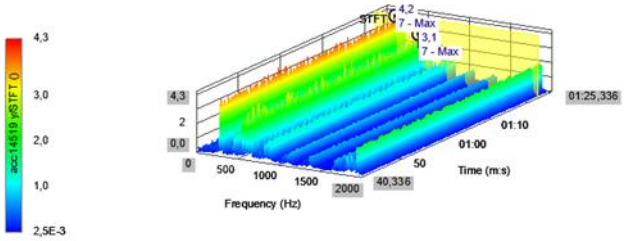

b)

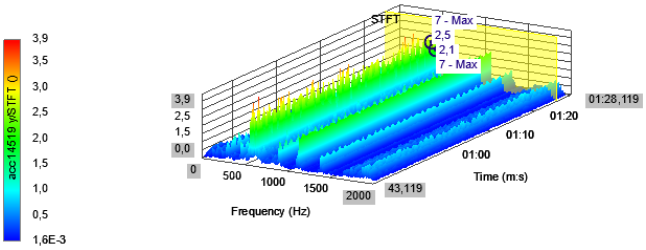

Fig. 30. STFT time-frequency analysis of the signals, measurement point 14519 in direction *y* for a constant load of 750 Nm (N): a) for clutch in locked operating mode, b) for clutch in flexible operating mode.

5. Conclusions

As a result of the application of the innovative highly flexible metal clutch in the drive system subject to the studies, and for the analysed cases of loads (500 ±250 Nm and 750 ±375 Nm), specific nature of torque variations (sinusoidal, triangular, rectangular, and constant), and different measurement points, with reference to the results depicted in:

- Figure 13 (direction *x*), it can be concluded that the largest average percentage increase in the RMS of vibration accelerations was 7.8% (Fig. 13a), and the largest average reduction thereof was multiple times greater, being as high as 30.1% (Fig. 13c);
- Figure 14, it can be concluded that the largest average percentage increase in the RMS of vibration accelerations for measurement axis *y*, where the largest vibration accelerations occurred, was 0.2% (Fig. 14b), while the largest average decrease thereof was significantly greater, being as much as 56.1% (Fig. 14c);
- Figure 15 (direction *z*), it can be concluded that the

largest average percentage increase in the RMS of vibration accelerations was 3.3% (Figure 15d), and the largest average reduction thereof was more than twice as great and amounted to 7.4% (Figure 15c);

- Figure 20 (axis *x*), it can be concluded that the largest average percentage increase in the peak-to-peak (P-P) of vibration accelerations was 1% (Fig. 20b), and the largest average reduction thereof was more than twenty times greater, being as high as 22.2% (Fig. 20c);
- Figure 21, it can be concluded that the largest average percentage increase in the peak-to-peak (P-P) of vibration accelerations for measurement axis *y*, where the largest vibration accelerations occurred, was 1.2% (Fig. 21b), while the largest average decrease thereof was several dozen times greater, being as much as 40.4% (Fig. 21c).

Following the studies and the frequency analysis addressed in this paper, with regard to measurement point 10244, where the RMS of vibration accelerations were the highest, for direction *y*, the relevant changes in the braking torque values, and the specific nature of the load torque changes (sinusoidal, rectangular, triangular, and constant), one can conclude that the maximum amplitude observed in the frequency spectrum always decreased as a result of the clutch operating in the flexible mode. The same outcome was obtained when analysing the second maximum amplitude observed within the frequency spectrum. Direction *y* was the one in which the RMS of the vibration accelerations prevailed in the case of the locked clutch operation at both measurement points and with all the given characteristics of the load torque variations. What can also be concluded is that, apart from one exception out of the 32 cases analysed, at that measurement point, the frequency values did not change significantly as a result of the flexible clutch operation (save for the case marked as 750/T/P).

The studies and time-frequency analyses conducted by the authors imply that placing the clutch in the flexible operating mode leads to changes in the time-frequency structure of the signals recorded at the measurement points analysed, and that, in many cases, this contributes to reducing the maximum instantaneous amplitudes of the STFT distribution.

To recapitulate on the above elaborations, it can be concluded that, during operation, the load torque of a drive system is subject to variations of diverse nature, including short periods of operation under a constant load, and therefore, with reference to the studies addressed in this paper, it has been demonstrated that it is possible to reduce the vibration accelerations in a drive system equipped with the proposed innovative highly flexible metal clutch while the system is operating under the conditions of a constant as well as time-varying load torque of different variation waveforms (sine, triangle, and rectangle). Reduction of vibrations benefits the durability and reliability of the drive system, and it should be highlighted that both during and after the testing, as well as over the course of the clutch disassembly, no alarming effects attributable to the excessive wear of the clutch components were detected, which could otherwise have a negative impact on its reliable operation.

Acknowledgments

This research was developed under project POIR.04.01.04-00-0081/17 entitled “Developing innovative scraper conveyors with increased start-up flexibility and extended service life,” co-financed by the National Centre for Research and Development in Poland.

References

1. Wang Y, Chen Q, Dai B, Wang D. Guidance and review: Advancing mining technology for enhanced production and supply of strategic minerals in China. Green and Smart Mining Engineering 2024; 1: 2–11, https://doi.org/10.1016/j.gsme.2024.03.005.
2. Doyle K, Moore K, Foster P. Criteria-driven socio-environmental maturity modelling for mining: driving positive sustainability attitudes and perceptions at diverse operational scales. Resources Policy 2025; 105: 105606, https://doi.org/10.1016/j.resourpol.2025.105606.
3. Onifade M, Zvarivadza T, Adebisi J A, Said K O, Dayo-Olupona O, Lawal A I, Khandelwal M. Advancing toward sustainability: The emergence of green mining technologies and practices. Green and Smart Mining Engineering 2024; 1: 157–174, https://doi.org/10.1016/j.gsme.2024.05.005.
4. Cimino A, Elbasheer M, Longo F, Mirabelli G, Solina V, Veltri P. Automatic simulation models generation in industrial systems:

A systematic literature review and outlook towards simulation technology in the Industry 5.0. Journal of Manufacturing Systems 2025; 80: 859–882, https://doi.org/10.1016/j.jmsy.2025.03.027.

5. Liu X , Zhang X, Wang L, Qu F, Shao A, Zhao L, Wang H, Yue X, Li Y, Yan W, He J. Research progress and prospects of intelligent technology in underground mining of hard rock mines. Green and Smart Mining Engineering 2024; 1: 12–26, https://doi.org/10.1016/j.gsme.2024.03.007.
6. Chatterjee Ch, Sindhwani R, Mangla S K, Hasteer N. Digitization of the mining industry: Pathways to sustainability through enabling technologies. Resources Policy 2025; 100: 105450, https://doi.org/10.1016/j.resourpol.2024.105450.
7. Crabbe M, Leader J, Hall H M, Burdett M. Technology adoption in the Canadian mining sector: A systematic scoping review. Resources Policy 2025; 103: 105566, https://doi.org/10.1016/j.resourpol.2025.105566.
8. Wen H, Liu M, Zhang D, Wang Z, Deng J, Wang W. HCl formation mechanism in the pyrolysis process of coal mine conveyor belt. Fuel 2025; 384: 133899, https://doi.org/10.1016/j.fuel.2024.133899.
9. Zhang D, Liu M, Wen H, Wang Z, Wang W, Kong X, Bing J. Study on the characteristics of gas phase products in coal mine conveyor belt fire. Thermochimica Acta 2024; 733: 179677, https://doi.org/10.1016/j.tca.2024.179677.
10. Liu X, Zhang X, Wang L, Qu F, Shao A, Zhao L, Wang H, Yue X, Li Y, Yan W, He J. Research progress and prospects of intelligent technology in underground mining of hard rock mines. Green and Smart Mining Engineering 2024; 1: 12–26, https://doi.org/10.1016/j.gsme.2024.03.007.
11. Yang X, Wu D, Chen H, Wang D. Study on the force chain characteristics with coal dust layer and the three-body contact stiffness. Particuology 2024; 92, https://doi.org/10.1016/j.partic.2024.05.014.
12. Wang X, Liang X, Tong S, Sun X. Influence of tempering temperature on microstructure and stress corrosion crack (SCC) behavior of a new high strength round-link chain steel. Corrosion Science 2025; 246: 112770, https://doi.org/10.1016/j.corsci.2025.112770.
13. Chen Y, Li W, Du Y X. Straightness measurement of conveyors based on SINS/UWB with a Robust Laplace Kalman filter. Measurement 2025; 249: 116978, https://doi.org/10.1016/j.measurement.2025.116978.
14. Li X, Xu Y, Liu J, Liu J, Pan G, Shi Z. A dynamic model for a shell-propulsion shaft system considering the shell and shaft flexibilities. Mechanical Systems and Signal Processing 2025; 224: 111928, https://doi.org/10.1016/j.ymssp.2024.111928.
15. Sun Y, Shi J, Wei Ch, Yang Y, Du M, Cao H. Dynamic modeling and vibration transmission analysis of the two-stage gearbox with simultaneous consideration of shaft flexibility and instantaneous gear meshing stiffness. Mechanical Systems and Signal Processing 2025; 225: 112272, https://doi.org/10.1016/j.ymssp.2024.112272.
16. Jiang F, Ding K, Zhang S, Wu Z, He G. Vibration response mechanism of fixed-shaft gear train with cracks based on rigid-flexible coupling dynamics and signal convolution model. Mechanical Systems and Signal Processing 2023; 198: 110417, https://doi.org/10.1016/j.ymssp.2023.110417.
17. Ma X, Li Z, Xiang J, Chen Ch, Huang F. Vibration characteristics of rotor system with coupling misalignment and disc-shaft nonlinear contact. Mechanical Systems and Signal Processing 2025; 223: 111839, https://doi.org/10.1016/j.ymssp.2024.111839.
18. Li T, Huang Z, Chen Z, Wang J, Wang Ch. Study on the torsional stiffness and vibration response law of laminated coupling considering the effect of excess. Mechanical Systems and Signal Processing 2025; 222: 111739, https://doi.org/10.1016/j.ymssp.2024.111739.
19. Li X, Xu Y, Liu J, Liu J, Pan G, Shi Z. Dynamic modelling of a floating spline-coupling shaft system with parallel misalignment and tooth backlash. Mechanical Systems and Signal Processing 2025; 226: 112363, https://doi.org/10.1016/j.ymssp.2025.112363.
20. Xu M, Han Y, Sun X, Shao Y, Gu F, Ball A D. Vibration characteristics and condition monitoring of internal radial clearance within a ball bearing in a gear-shaft-bearing system. Mechanical Systems and Signal Processing 2022; 165: 108280, https://doi.org/10.1016/j.ymssp.2021.108280.
21. Deng S, Shen J, Yang C, Qian D, Hua L. Influence of various balls and groove curvature radii on dynamic stiffness of ball bearings based on nonlinear dynamic model. Applied Mathematical Modelling 2024; 127: 259–280, https://doi.org/10.1016/j.apm.2023.12.010.
22. Shah D S, Patel V N. A dynamic model for vibration studies of dry and lubricated deep groove ball bearings considering local defects on races. Measurement 2019; 137: 535–555, https://doi.org/10.1016/j.measurement.2019.01.097.
23. Yue K, Wang L, Zhang H, Huang W, Du M, Chen Z. A novel model for analyzing meshing characteristics in a non-uniformly distributed gear system with irregular tooth edge spalling fault. Mechanical Systems and Signal Processing 2025; 230: 112657,

https://doi.org/10.1016/j.ymssp.2025.112657.
24. Yuan B, Wang J, Han B, Xiong X, Dong H. A novel mathematical model to capture the 3D dynamic contact state of gear pairs considering system flexibility. Mechanism and Machine Theory 2025; 209: 105999, https://doi.org/10.1016/j.mechmachtheory.2025.105999.
25. Yang S, Zhu C, Li C, Zhou Y, Wang W, Wang S. Novel dynamic modeling and analysis method of the wind turbine gearbox gear-bearing coupling system considering gear crack and tooth modification with support shaft flexibility. Mechanism and Machine Theory 2025; 212: 106058, https://doi.org/10.1016/j.mechmachtheory.2025.106058.
26. Margielewicz J, Gąska D, Wojnar G. Numerical modelling of toothed gear dynamics. Scientific Journal of Silesian University of Technology. Series Transport 2017; 97: 105-115. ISSN: 0209-3324, https://doi.org/10.20858/sjsutst.2017.97.10.
27. Juzek M, Wojnar G. Analysis of stresses and deformations of a gear with modified internal structure. Projektowanie, badania i eksploatacja / Rysiński J. (red.), Monography, 2021, Akademia Techniczno-Humanistyczna w Bielsku-Białej, s.115-122, ISBN 978-83-66249-83-7, https://doi.org/10.53052/9788366249837.09.
28. Hao Z, Wang D, Zhang Q, Wang S, Wu Y, Shi X, Li W. Vibration characteristic analysis of a two-stage spur gear transmission system with tooth crack and profile shifted. Journal of Sound and Vibration 2025; 615: 119211, https://doi.org/10.1016/j.jsv.2025.119211.
29. Łazarz B, Wojnar G, Czech P. Early fault detection of toothed gear in exploitation conditions. Maintenance and Reliability 2011; 1.
30. Tupkar R, Kumar D, Sakhale Ch. Material selection and parametric evaluation for medium duty belt conveyor: A review on current status and future directions. Materials Today: Proceedings 2024, https://doi.org/10.1016/j.matpr.2024.04.021.
31. Suchoń J. Górnicze przenośniki zgrzebłowe. Teoria, badania i eksploatacja. Instytut Techniki Górniczej KOMAG, Gliwice 2012.
32. Angeles E, Kumral M. Optimal inspection and preventive maintenance scheduling of mining equipment. Journal of Failure Analysis and Prevention 2020; 20: 1408–1416, https://doi.org/10.1007/s11668-020-00949-z.
33. Juzek M, Pisuła J, Žuľová L. Extended analysis of selected deviations and precision of gears manufacturing as a possibility for reduction of gearboxes' vibroactivity used in means of transport. Scientific Journal of Silesian University of Technology. Series Transport 2025; 126: 65-78. ISSN: 0209-3324, https://doi.org/10.20858/sjsutst.2025.126.4.
34. Wieczorek A N, Konieczny Ł, Wojnar G, Wyroba R, Filipowicz K, Kuczaj M. Reduction of dynamic loads in the drive system of mining scraper conveyors through the use of an innovative highly flexible metal coupling. Eksploatacja i Niezawodnosc – Maintenance and Reliability 2024, 26 (2): art. no. 181171, https://doi.org/10.17531/ein/181171.
35. Homišin J, Kaššay P, Urbanský M, Puškár M, Grega R, Krajňák J. Electronic constant twist angle control system suitable for torsional vibration tuning of propulsion systems. J. Mar. Sci. Eng. 2020; 8(9): 721, https://doi.org/10.3390/jmse8090721.
36. Grega R, Krajnak J, Žul'ová L, Kaˇcír M, Kaššay P, Urbanský M. innovative solution of torsional vibration reduction by application of pneumatic tuner in shipping piston devices. J. Mar. Sci. Eng. 2023; 11, 261, https://doi.org/10.3390/jmse11020261.
37. Krajnak J, Homisin J, Grega R, Kassay, P, Urbansky, M. The failures of flexible couplings due to self-heating by torsional vibrations - validation on the heat generation in pneumatic flexible tuner of torsional vibrations. Engineering Failure Analysis 2021; vol. 119: 104977, https://doi.org/10.1016/j.engfailanal.2020.104977.
38. Wieczorek A N. Własności eksploatacyjne metalowych sprzęgieł podatnych do korytarzowych przenośników zgrzebłowych. 2024, 25. Międzynarodowa Konferencja Naukowo-Techniczna KOMTECH „Górnictwo w dobie zielonej transformacji" 2024 - report presented.
39. Kowal A, Filipowicz K. The construction of metal flexible torsional coupling. Transport Problems 2007; 2: 73-80.
40. Filipowicz K. Dwukierunkowe metalowe sprzęgła podatne skrętnie. Gliwice, Wydawnictwo Politechniki Śląskiej 2011.
41. Adamiak B, Andrych-Zalewska M, Merkisz J, Chłopek Z. The uniqueness of pollutant emission and fuel consumption test results for road vehicles tested on a chassis dynamometer. Eksploatacja i Niezawodność – Maintenance and Reliability. 2025; 27(1), https://doi.org/10.17531/ein/195747.
42. Karpenko M, Ževžikov P, Stosiak M, Skačkauskas P, Borucka A, Delembovskyi M. Vibration Research on Centrifugal Loop Dryer Machines Used in Plastic Recycling Processes. Machines. 2024; 12(1):29, https://doi.org/10.3390/machines12010029.
43. Rychlik A, Vrublevskyi O, Prokhorenko A. Modelling of the diagnostic station operation process to identify damage to the wheel rim structure. Journal of Mechanical Science and Technology 2019; vol. 33, 4129–4138, https://doi.org/10.1007/s12206-019-0808-x.